




Cite this: *New J. Chem.*, 2018, 42, 4661

Electrodeposition of Ni–Mo–rGO composite electrodes for efficient hydrogen production in an alkaline medium†

Sandhya Shetty, M. Mohamed Jaffer Sadiq, D. Krishna Bhat and A. Chitharanjan Hegde *

The mechanism and kinetics of the hydrogen evolution reaction (HER) on Ni–Mo–rGO composite electrodes in 1.0 M KOH solution were investigated by cyclic voltammetry (CV), chronopotentiometry (CP) and potentiodynamic polarization techniques. Ni–Mo–rGO composite coatings were deposited on a copper substrate by an electrodeposition method at a current density (c.d.) ranging from 1.0 to 4.0 A dm⁻². The change in surface morphology and chemical composition was characterized by scanning electron microscopy (SEM), X-ray diffraction (XRD) analysis, energy dispersive X-ray (EDX) analysis and X-ray photoelectron spectroscopy (XPS). It was shown that the carbon content of the composite coatings was affected by c.d. With the increase in the carbon content in the Ni–Mo–rGO composite coatings, the onset potential was decreased and the exchange current density was increased during the HER. The minimum onset potential and maximum exchange current density of Ni–Mo–rGO composite coatings for the HER were –401.6 mV and 4.31 μA cm⁻². The best composite coating exhibited a maximum peak current density of –0.517 A cm⁻² at –1.6 V, which is approximately 3 times better than that of the binary Ni–Mo alloy, indicating the best activity for hydrogen production. The potentiodynamic polarization measurements revealed that composite coatings are much more resistant to corrosion than binary alloy coatings.

Received 22nd November 2017,
Accepted 12th February 2018

DOI: 10.1039/c7nj04552b

rsc.li/njc

Introduction

As a result of public awareness of serious environmental threats caused by massive utilization of fossil and nuclear fuels, an agreement has been reached towards an energetic system based on clean, sustainable and renewable resources.¹ Hydrogen is considered as an alternative clean energy source of fossil fuels and an ideal energy resource for the future.² Even though hydrogen is the most abundant element in the universe, it cannot be found in the pure state in nature. In this regard, production of low cost and environmentally clean hydrogen by means of renewable energy sources becomes very important. Water is a renewable resource of great interest for hydrogen production and water electrolysis represents the most important path to obtain hydrogen from water, although thermal and photocatalytic decompositions are also attracting some attention. It is an advanced technology based on the generation of hydrogen and oxygen from water molecules which are dissociated by applying direct current electric energy. The hydrogen obtained with this

technology has a high purity that can reach 99.99% when oxygen and vapor are removed from the hydrogen produced.³ From a technological point of view, at present, one of the most mature and effective methods for hydrogen production is alkaline water electrolysis. However, the main problem with electrolytic hydrogen production is the low electrode catalytic efficiency and high energy consumption. Ni-based alloys have long been recognized as suitable electrode materials for hydrogen evolution reaction (HER) due to their relatively high catalytic activity and low cost.^{4–6} Although nickel shows a high initial electrocatalytic activity towards the HER, it experiences extensive deactivation as a cathode during alkaline water electrolysis. The alloying of two (or more) metals has long appeared as the most straightforward approach to achieve electrocatalytic activity for the HER.⁷ Among them, the Ni–Mo binary alloy either electrodeposited,⁸ mechanically alloyed,⁹ or thermally prepared¹⁰ shows superior electrocatalytic performance for the HER. The enhanced activity corresponds to a synergistic effect due to the electron-transfer between electron-rich Ni and electron-deficient Mo in the Ni–Mo alloy.^{11,12}

Efforts to develop highly active and efficient electrocatalysts for electrolytic hydrogen production have been a long-standing challenge. In general, the efficiency of the electrode materials can be improved by increasing the real surface area or increasing

Department of Chemistry, National Institute of Technology Karnataka, Srinivasnagar, 575025, Surathkal, India. E-mail: acrhegde@gmail.com; Fax: +91-824-2474033; Tel: +91-9980360242

† Electronic supplementary information (ESI) available. See DOI: 10.1039/c7nj04552b

the intrinsic catalytic activity by a synergistic combination of multicomponents.¹³ Nowadays, graphene, an emerging two-dimensional structure of free-standing carbon atoms which are packed into a honeycomb-like crystal structure, is being predicted to have numerous potential applications because of its unusual electron transport properties and other distinct characteristics. Also, graphene-based materials possess large specific surface area, excellent conductivity and availability for surface functionalization, which are important characteristics for electrochemical applications.¹⁴ The high conductivity of graphene makes it an inexpensive alternative to CNTs (carbon nanotubes).¹⁵ Because of the planar structure of graphene, both sides of the graphene sheets could be utilized as a support for catalysts.¹⁶ These properties make graphene a promising and favorable catalyst support.¹⁷

In the present work, electrodeposition of Ni–Mo alloys along with reduced graphene oxide (rGO) is carried out on a copper substrate of a known surface area. The rGO can facilitate charge transfer and ionic interchange to enhance electrocatalysis.^{18,19} The enhancement of its electrocatalytic efficiency is studied using electrochemical techniques such as CV and CP in 1.0 M KOH medium. Furthermore, the potentiodynamic polarization technique is used to study the stability of the electrocatalysts in the same alkaline medium. Additionally, corrosion rates and HER mechanism pathway are determined using the parameters derived from the Tafel curves.

Experimental

Synthesis of reduced graphene oxide (rGO)

Graphene oxide was synthesized using the modified Hummers method. In brief, natural graphite flasks (1.0 g) and NaNO₃ (0.5 g) were mixed homogeneously in a 250 mL beaker, with the simultaneous addition of concentrated H₂SO₄ (50 mL) under constant mechanical stirring. KMnO₄ (3.0 g) was then added slowly to the above mixture and stirred at a constant room temperature (25 °C) for 1 hour. Later, distilled water (75 mL) was added to the mixture and continuously stirred for 30 minutes at 95 °C. Finally, the mixture of distilled water (100 mL) and H₂O₂ (1.0 mL) was consequently added to terminate the reaction, at this stage the color of the reaction suspension turned from brown to yellow. The obtained graphite oxide suspension was separated by centrifugation, washed with distilled water, and further sonicated to get a graphene oxide solution. The rGO was finally synthesized by a microwave irradiation method. The resultant graphene oxide solution was then irradiated with microwave radiation at 350 W for 10 minutes; here the color of the reaction suspension turned black. The obtained black precipitate of rGO was separated by filtration, washed several times with distilled water and dried at 80 °C for 12 hours in a vacuum to obtain the rGO powder.

Electrodeposition of Ni–Mo–rGO composite coatings

The electrodeposition of the Ni–Mo–rGO electrocatalyst was accomplished on a copper substrate from an alkaline sulfate

Table 1 Composition and deposition conditions of the optimized Ni–Mo–rGO electrolyte bath

Bath constituents	Amount (g L ⁻¹)	Operating parameters
NiSO ₄ ·6H ₂ O	18	Anode: Ni plate
Na ₂ MoO ₄	48	Cathode: copper
Na ₃ C ₆ H ₅ O ₇	105	pH: 9.5
rGO	0.5	Temperature: 303 K
		Deposition time: 600 s
		Current density: 1.0–4.0 A dm ⁻²

bath with composition and operating parameters as given in Table 1. The electrolytic bath was prepared from analytical grade reagents (Merck, India) using double distilled water. Ni–Mo–rGO composite coatings are deposited on copper plates, and a copper rod (both having same specifications) of known surface area, depending on the requirements. For characterization purposes, composite coatings are deposited on copper plates (7.5 cm × 2.5 cm × 0.2 cm) in a 200 mL capacity cubic cell (made of PVC material).

All the electrochemical and electrocatalytic studies of the electrodeposited Ni–Mo–rGO coatings on a cross-sectional area of the copper rod were carried out in a customized glass cell (250 mL capacity) and the results are given in ESI† data (Fig. S1). The copper rod was sealed with Teflon tape, leaving an area of 1.0 cm² exposed for electrodeposition and the same surface is subjected to the electrochemical test in 1.0 M KOH solution. The mirror polished copper surface was degreased using trichloroethylene, electro-cleaned and pickled in 1:1 HNO₃ to activate the surface prior to deposition and finally rinsed with distilled water. A copper substrate is used as the cathode in the electrochemical cell and a pure nickel plate of the same exposed surface area is used as an anode and kept parallel at a 5 cm distance from each other. 0.5 g L⁻¹ of synthesized rGO was added into the Ni–Mo bath. The bath was agitated ultrasonically for 2 hours to ensure uniform dispersion of rGO. An Agilent N6705A DC power analyzer was used as a highly sensitive power source for electrodeposition. The total time for electrodeposition was fixed at 600 s in all the cases for optimal comparison.

Electrochemical measurements

An electrocatalytic study of Ni–Mo alloy and Ni–Mo–rGO composite coatings was carried out using a customized three-electrode tubular glass cell, with arrangements as shown in Fig. 1. This electrochemical cell was designed for the quantitative measurement of hydrogen gas liberated, when the electrodeposited Ni–Mo–rGO composite electrode was subjected to cathodic polarization. The prepared Ni–Mo–rGO samples developed at the different c.d.'s on a copper rod with an exposed geometric surface area of 1.0 cm² were used as the working electrode, a saturated calomel electrode (SCE) was used as the reference electrode and platinum was used as the counter electrode. All the potentials mentioned in this paper are relative to SCE which is 0.241 V positive to the standard hydrogen electrode. Luggin's capillary with the agar–KCl salt bridge was used to minimize the error due to ohmic drop. The cell is also fitted with graduated tubes (burette), which collects

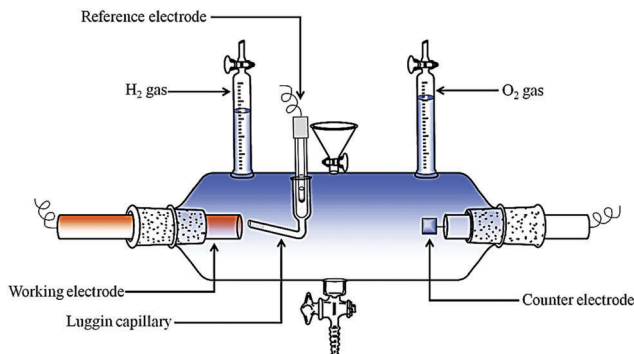


Fig. 1 Experimental setup used for evaluating the electrocatalytic performance of Ni–Mo alloy and Ni–Mo–rGO composite coatings, with provision to collect liberated H₂ and O₂ gas.

the volume of liberated gas (hydrogen and oxygen) displacing the solution, whose volume could easily be measured.

Cyclic voltammetry (CV), potentiodynamic polarization and chronopotentiometry (CP) techniques were used to characterize the electrochemical performance of the deposited electrodes in 1.0 M KOH solution at room temperature. All the measurements were performed with a computer-controlled electrochemical system (model IVIUM, VERTEX, Netherlands). The potentiodynamic polarization study was carried out by polarizing the test electrode by subjecting it to a potential drift -250 mV cathodically and $+250$ mV anodically relative to the OCP at a scan rate of 1 mV s⁻¹ and the corresponding Tafel curves were recorded in alkaline solution, respectively. From Tafel extrapolation, the polarization parameters such as corrosion potential (E_{corr}), corrosion current density (i_{corr}), corrosion rate (CR) and cathodic Tafel slope (β_c) were deduced.

Characterization

The morphology, as well as the composition of the coatings, was characterized using a scanning electron microscope (SEM, EVO 18 from Carl Zeiss, Germany) equipped with EDX. The crystal structure was measured by an X-ray diffractometer (XRD, Rigaku Miniflex 600), using Cu K α ($\lambda = 1.5406$ Å) radiation, in a continuous scan mode at the scan rate of 2° min⁻¹. The chemical states of the elements in the as-synthesized samples were recorded by using X-ray photoelectron spectroscopy (XPS, Kratos XSAM 800) using monochromatic Al-K α radiation. All the measurements were performed after 10 min of argon ion sputtering to avoid the influence of oxidation by air and were referenced to the C (1s) line binding energy of 284.5 eV.

Results and discussion

SEM analysis

The surface morphology of the Ni–Mo alloy coatings deposited at different c.d.'s (*i.e.* 1.0–4.0 A dm⁻²) was previously reported in the literature by our group.²⁰ With the addition of graphene to the deposition bath, as expected, a change in surface morphology of the coatings was observed. As seen from Fig. 2, an apparent hybrid structure is successfully produced. Nanoparticles are

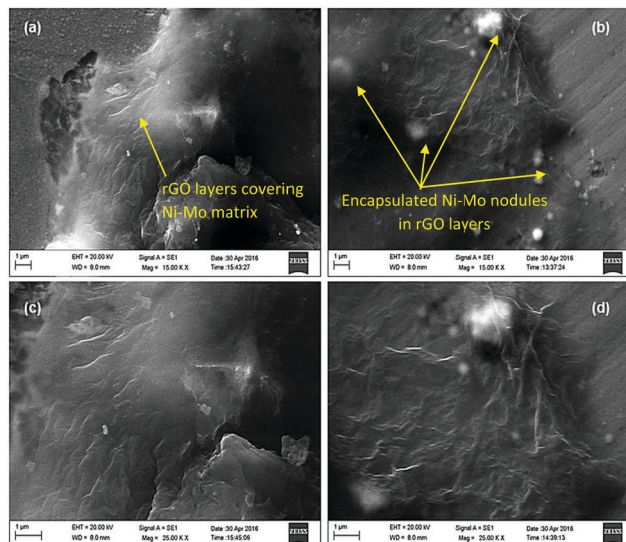


Fig. 2 SEM images of the Ni–Mo–rGO composite coatings deposited from the optimal bath at (a) 1.0 A dm⁻² and (b) 4.0 A dm⁻² displaying irregularly shaped graphene layers embedded in the Ni–Mo alloy matrix; (c and d) are magnified images showing layers of graphene and encapsulated alloy nodules in the graphene network.

well dispersed on or covered under the rGO sheets. It can be observed that the size of the nodules increases with the increase in c.d. but they become few in number. Owing to the high specific surface area of graphene, the adsorption of the electrolyte onto the surface is expected to be very high. On applying current, the electrolyte adsorbed graphene gets dragged towards the cathode and gets incorporated into it along with the growing alloy layer. The adsorbed metal ions on the graphene are reduced into metal atoms and deposit as an encapsulated bundle of alloy particles within the graphene network (Fig. 2(b)). Such structural changes due to the addition of graphene increase the surface roughness and hence increase the electroactive surface area of the composite coating, which in turn enhances its electrocatalytic activity. The observation of such structural changes due to the addition of graphene is of great importance in understanding its significance in enhancing the electrocatalytic activity of the binary alloy coatings.²¹

EDX analysis

EDX analysis was carried out to determine the presence of different elements in the coatings. The composition of the composite coatings is shown in Table 2 and the spectrum is given in the ESI† (Fig. S2). From the data reported in Table 2, it is clear that c.d. has a great influence on the composition of the coatings. Also, the Ni–Mo–rGO coating prepared at 4.0 A dm⁻² contains the maximum carbon content 16.14% when compared with the coatings deposited at lower c.d.'s.

It is well known that molybdenum in the metallic state cannot be electrodeposited separately from an aqueous solution,²² but it can be co-deposited with ferrous metals forming an alloy. This phenomenon is so-called induced co-deposition.²³ In the induced co-deposition, the behavior of individual metal is irregular and

Table 2 Elemental composition of Ni–Mo–rGO coatings deposited at different c.d.'s from the optimal bath

Coating configuration	wt% Ni	wt% Mo	wt% C
(Ni–Mo–rGO) _{1.0 A dm⁻²}	49.36	42.08	8.56
(Ni–Mo–rGO) _{2.0 A dm⁻²}	50.10	38.05	11.85
(Ni–Mo–rGO) _{3.0 A dm⁻²}	54.54	32.03	13.43
(Ni–Mo–rGO) _{4.0 A dm⁻²}	57.55	26.31	16.14

difficult to predict, which reflects the complicated mechanism of alloy formation. During this process, the discharge of Ni(II) and Mo(VI) complex ions and hydrogen evolution occur on the cathode at the same time. However, besides the induced co-deposition of metallic molybdenum, low valence state oxides of molybdenum reduced from Mo(VI) may exist in the deposited films.^{24,25} Furthermore, the bath exhibits a very low partial current density for the deposition of Mo (compared to its calculated limiting current density), due to a low rate of mass transport of electroactive species (Mo²⁺ ions) from a pH-dependent molybdate–citrate complex. Hence, an unusual decrease of Mo content with c.d. is more due to changes in pH (due to the evolution of H₂ gas), responsible for shifting the equilibrium of its citrate complex, than due to the change in its limiting current density.²⁶ This unusual change of composition with the c.d. is a specific nature of the induced co-deposition of Ni–Mo alloy as observed by Bratoeva *et al.*²⁷

XPS analysis

XPS analysis was also performed to determine the chemical states of the elements in the Ni–Mo–rGO and Ni–Mo alloy

deposits which are very important for the electrochemical and catalysis behavior. Fig. 3(a–d) displays the chemical composition and states of the Ni–Mo–rGO and Ni–Mo coatings. From the survey spectrum (Fig. 3(a)) the presence of C, O, Ni and Mo peaks was observed. The high-resolution Ni (Fig. 3(b)) XPS spectra show the binding energies of Ni 2p_{3/2} (+2 = 852.2, +3 = 855.6) and Ni 2p_{1/2} (+2 = 869.4, +3 = 873.3) for Ni–Mo–rGO, and Ni 2p_{3/2} (+2 = 852.6, +3 = 855.9) and Ni 2p_{1/2} (+2 = 869.8, +3 = 873.7) for Ni–Mo and its satellite, respectively. The high-resolution Mo (Fig. 3(c)) XPS spectra show the binding energies of Mo 3d_{3/2} (+6 = 235.2, +2 = 230.7) and Mo 3d_{5/2} (+6 = 232.1, +2 = 227.7) for Ni–Mo–rGO, and Mo 3d_{3/2} (+6 = 235.6, +2 = 231.1) and Mo 3d_{5/2} (+6 = 232.4, +2 = 228) for Ni–Mo, respectively. However, from the peak positions it is observed that the Ni and Mo binding energy peak in Ni–Mo–rGO is negatively shifted as compared to the Ni–Mo sample ($\Delta E = 0.3\text{--}0.4$ eV) (Fig. 3(b) and (c)), indicating the existence of an electron transfer process between the Ni–Mo and rGO networks, which is beneficial for increasing the catalytic activity and also favorable for stabilizing the electronic and ionic conductivity. A high-resolution spectrum of C 1s shows the peak located at 284.7 eV, which corresponds to the carbon of the rGO (Fig. 3(d)).

XRD study

XRD was used for the structural characterization of the Ni–Mo–rGO composite coatings. The obtained diffraction patterns are shown in Fig. 4. As observed in Fig. 4, the peaks at 22.3°, 43.3°, 50.4°, 74.03° and 89.8° are the characteristic peaks of the tetragonal MoNi₄ phase (JCPDS no. 03-065-1533), and correspond to the

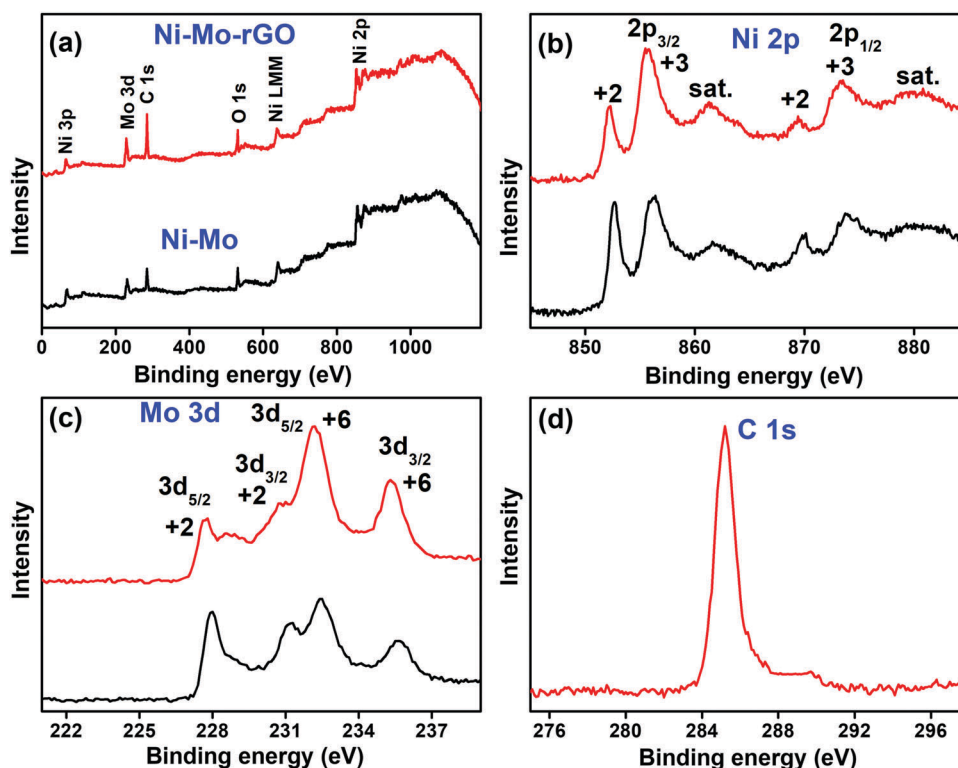


Fig. 3 Survey spectrum (a) and high-resolution spectrum of Ni 2p (b), Mo 3d (c) and C 1s (d) of the Ni–Mo–rGO and Ni–Mo coatings.

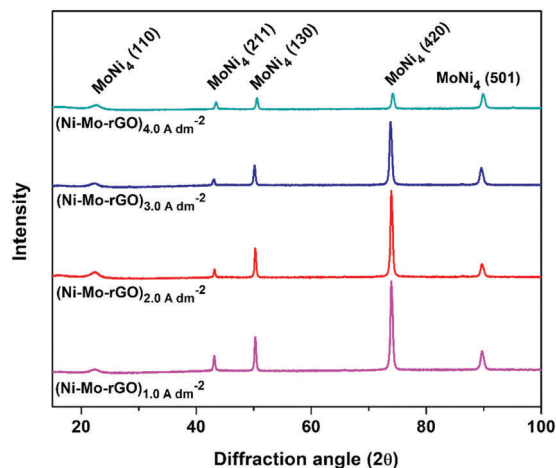


Fig. 4 XRD patterns of the Ni-Mo-rGO composite coatings deposited at different c.d.'s.

(110), (211), (130), (420) and (501) planes.²⁸ As seen from the XRD patterns, there were no apparent reflections of rGO; this could be ascribed to the lower percentage of rGO in the coatings. The grain size was obtained from the XRD line broadening analysis of the peaks using the Scherrer equation,²⁹

$$d = \frac{0.9\lambda}{\beta \cos \theta} \quad (1)$$

where d is the crystallite size, λ is the wavelength of X-ray radiation, β is the full-width half maxima (FWHM) of the diffraction peak and θ is the diffraction angle. Upon calculation, the average crystallite size of the coatings was found to be 25 nm.

A comparison of the diffraction patterns of the Ni-Mo alloy coating and Ni-Mo-rGO composite coating deposited at 4.0 A dm⁻² is given in Fig. 5. From the graph, it is evident that there are no significant changes in the crystallographic orientation after the addition of rGO; however, the intensity of the (420) plane is reduced substantially indicating the reduction in

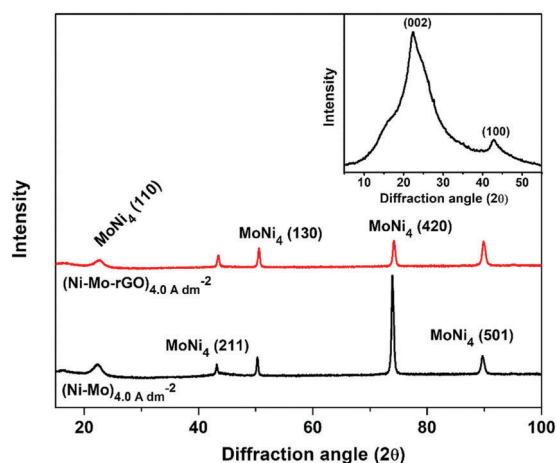


Fig. 5 XRD patterns of the Ni-Mo alloy and Ni-Mo-rGO composite coatings deposited at 4.0 A dm⁻², along with the XRD pattern of rGO shown in the inset.

Table 3 Scherrer's equation parameters of Ni-Mo and Ni-Mo-rGO composite coatings

Coating configuration	θ	hkl plane	FWHM	d (nm)
(Ni-Mo) _{4.0 A dm⁻²}	73.90	420	0.3361	29.6
(Ni-Mo-rGO) _{4.0 A dm⁻²}	74.13	420	0.4137	24.1

its crystallinity. The values of the Scherrer parameters for the (420) plane of Ni-Mo and Ni-Mo-rGO composite coatings are given in Table 3. The crystallite size of the (420) plane of the composite coating was 24.1 nm against the 29.6 nm of the Ni-Mo alloy coating. This reduction in the crystallite size of the composite coating was further supported by a higher peak width in their diffractograms. This increase in peak width of composite coating exhibits the influence of graphene on the Ni-Mo coating. During the deposition of the composite coating, the incorporation of graphene into the matrix enhances the nucleation by creating disorder. The diffusion of graphene towards the growth centers on the surface caused a detrimental effect on the crystal growth. This increase in the nucleation growth and retardation in the crystal growth is responsible for the reduction of the crystal size.¹⁴

Potentiodynamic polarization study

To evaluate the suitability of the Ni-Mo-rGO composite electrode for possible industrial application, the electrochemical stability of the electrode was investigated using a potentiodynamic polarization study. The corrosion behavior of the Ni-Mo-rGO coatings was evaluated using the Tafel plots. Fig. 6 shows the Tafel curves of the Ni-Mo-rGO composite coatings, and the CRs of the coatings, deposited at different c.d.'s, are reported in Table 4. From the corrosion data, it can be inferred that the Ni-Mo-rGO composite coating deposited at 4.0 A dm⁻² (having about 57.6% Ni) shows the least CR, *i.e.* 4.69×10^{-2} mm year⁻¹, while the coatings deposited at lower c.d.'s are more susceptible to corrosion.

Fig. 7 compares the Tafel curves of the Ni-Mo alloy and Ni-Mo-rGO composite coatings recorded under electrocatalytic

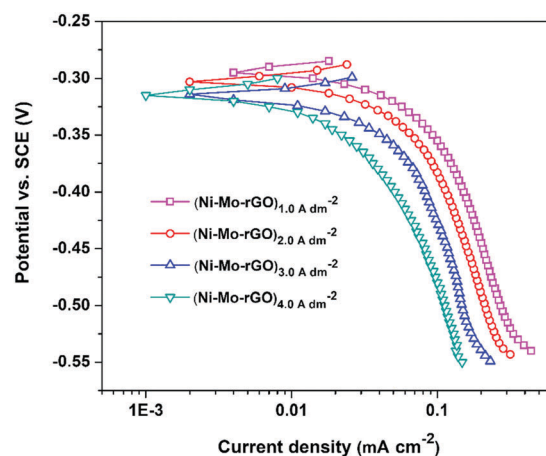


Fig. 6 Potentiodynamic polarization curves of Ni-Mo-rGO composite coatings deposited at different c.d.'s.

Table 4 Corrosion parameters such as E_{corr} , i_{corr} and CR's for the Ni–Mo–rGO composite coatings deposited at different c.d.'s, using the same optimal bath

Coating configuration	$-E_{\text{corr}}$ (V vs. SCE)	i_{corr} ($\mu\text{A cm}^{-2}$)	CR $\times 10^{-2}$ (mm year $^{-1}$)
(Ni–Mo–rGO) $_{1.0 \text{ A dm}^{-2}}$	0.290	21.50	12.56
(Ni–Mo–rGO) $_{2.0 \text{ A dm}^{-2}}$	0.298	19.61	10.28
(Ni–Mo–rGO) $_{3.0 \text{ A dm}^{-2}}$	0.311	15.36	7.80
(Ni–Mo–rGO) $_{4.0 \text{ A dm}^{-2}}$	0.315	9.91	4.69

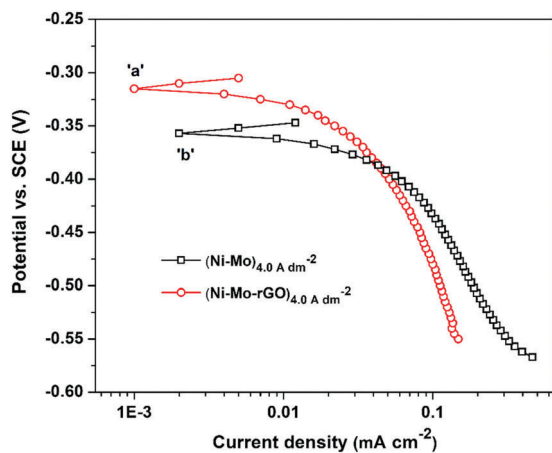


Fig. 7 Comparison of Tafel curves of the Ni–Mo alloy and Ni–Mo–rGO composite coatings developed at 4.0 A dm^{-2} .

working conditions. It can be observed from Fig. 7 that curve 'a' is shifted to a more positive potential compared to curve 'b' indicating the more noble character of the Ni–Mo–rGO composite coating and also its i_{corr} value decreased significantly relative to the Ni–Mo alloy deposit. This shift of E_{corr} and a decrease in i_{corr} indicates the higher corrosion resistance property of the composite coatings.

In order to decouple the chemical composition related intrinsic activity of the Ni–Mo–rGO composites towards hydrogen evolution, the effective exchange current density, i_0 , for the Ni–Mo–rGO electrodes was calculated. The i_0 is derived directly from the intercept by the extrapolation of the Tafel slope to the equilibrium potential based on its relationship with the overpotential described as:³⁰

$$\eta = a + b \log i \quad (2)$$

where η (V) represents the applied overpotential, i (A cm^{-2}) the resulting (measured) current, b (V dec^{-1}) the Tafel slope and a (V) the intercept related to i_0 (A cm^{-2}) through equation $a = (2.3RT)/(\beta nF) \times \log i_0$.

The optimal HER electrocatalyst is the material that gives the highest current at the least overpotential and this particular electrocatalyst shows low β_c and large i_0 values. The kinetic parameters of the Tafel curves are given in Table 5. As seen from the data given in Table 5, the i_0 values decrease with the c.d. and are found to be maximum for the composite, coated at 1.0 A dm^{-2} indicating the better efficiency of that electrode for the highest HER activity. Furthermore, values of β_c that were

Table 5 Kinetic parameters obtained from the cathodic polarization curves for the HER on the Ni–Mo–rGO composite coatings developed at different c.d.'s

Coating configuration	$-\beta_c$ (mV dec^{-1})	i_0 ($\mu\text{A cm}^{-2}$)	$-\eta_c$ (mV vs. SCE)
(Ni–Mo–rGO) $_{1.0 \text{ A dm}^{-2}}$	89	4.31	401.6
(Ni–Mo–rGO) $_{2.0 \text{ A dm}^{-2}}$	95	4.11	409.9
(Ni–Mo–rGO) $_{3.0 \text{ A dm}^{-2}}$	98	3.92	419.5
(Ni–Mo–rGO) $_{4.0 \text{ A dm}^{-2}}$	103	3.78	426.6

Table 6 Comparison of Tafel slope (β_c) exchange current density (i_0) and cathodic overpotential (η_c) of Ni–Mo alloy and Ni–Mo–rGO composite coatings deposited at 1.0 A dm^{-2} and 4.0 A dm^{-2}

Coating configuration	$-\beta_c$ (mV dec^{-1})	i_0 ($\mu\text{A cm}^{-2}$)	$-\eta_c$ (mV vs. SCE)
(Ni–Mo) $_{1.0 \text{ A dm}^{-2}}$	115	3.18	438.8
(Ni–Mo) $_{4.0 \text{ A dm}^{-2}}$	120	2.49	451.2
(Ni–Mo–rGO) $_{1.0 \text{ A dm}^{-2}}$	89	4.31	401.6
(Ni–Mo–rGO) $_{4.0 \text{ A dm}^{-2}}$	103	3.78	426.6

directly obtained from the slopes of the Tafel curves increase with the increase in c.d. This signifies a better electrocatalytic behavior for the HER by the coatings developed at lower c.d. (1.0 A dm^{-2}), as it was found to have the least β_c and highest i_0 value. A lower Tafel slope means that a catalyst requires a low applied overpotential to generate a required current. Since i_0 is the measure of electron transfer rate of a catalyst,³¹ a higher amount of i_0 means a higher electrocatalytic activity,³² further proving the point.

From Table 6, it can be seen that the i_0 for HER on the Ni–Mo–rGO electrodes is obviously higher than that on the Ni–Mo electrodes, showing that the intrinsic activity of the Ni–Mo–rGO composite coating toward HER is remarkably higher than that of the Ni–Mo alloy coating. This suggests that the introduction of rGO into the Ni–Mo alloy coating enhances its intrinsic electrocatalytic activity for the HER in addition to an increase in the surface area.¹³

Cyclic voltammetry

The electrocatalytic activity of the Ni–Mo–rGO composite coating deposited over the c.d. range of 1.0 A dm^{-2} to 4.0 A dm^{-2} for the HER has been evaluated using the CV technique in the potential range of 0.0 V to -1.6 V at a scan rate of 50 mV s^{-1} for 50 cycles. It was observed that the initial cycles showed larger cathodic peak current density (i_{pc}) values which eventually decreased with the increase in the number of cycles. After about 25 cycles, the value of i_{pc} was found to be constant, and the CV curves were observed to retrace the previous cycle. This situation corresponds to the conditions under which the rate of adsorption of the H atom on the surface for the formation of H_2 gas is equal to the rate of desorption of H_2 gas.³³ The CV curves for the HER of the Ni–Mo–rGO composite coatings are shown collectively in Fig. S3 (ESI[†]) and the corresponding electrochemical parameters are listed in Table 7.

From the data in Table 7, it is evident that i_{pc} decreases with the increase in c.d. It can be observed that the Ni–Mo–rGO composite coatings developed at the lowest c.d. (1.0 A dm^{-2})

Table 7 HER parameters of Ni–Mo–rGO coatings developed at different c.d.'s from the optimal bath

Coating configuration	Cathodic peak c.d. (i_{pc}) ($A\ cm^{-2}$)	Onset potential for HER (V vs. SCE)	Volume of H_2 evolved in 300 s (cm^3)
(Ni–Mo–rGO) $_{1.0\ A\ dm^{-2}}$	–0.517	–1.06	15.7
(Ni–Mo–rGO) $_{2.0\ A\ dm^{-2}}$	–0.407	–1.09	14.4
(Ni–Mo–rGO) $_{3.0\ A\ dm^{-2}}$	–0.314	–1.11	13.2
(Ni–Mo–rGO) $_{4.0\ A\ dm^{-2}}$	–0.222	–1.14	12.3

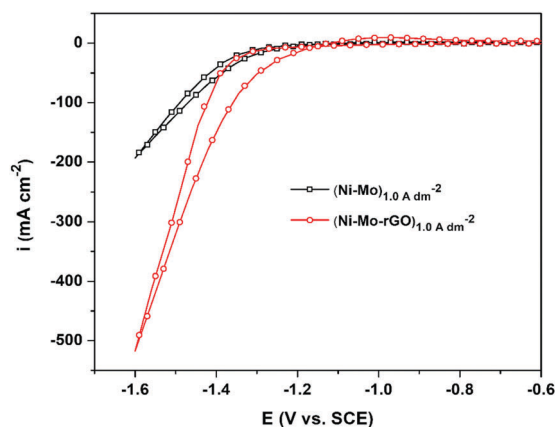


Fig. 8 Comparison of CV curves for HER on the surface of the Ni–Mo alloy and Ni–Mo–rGO composite coatings deposited at same c.d. ($1.0\ A\ dm^{-2}$).

show the maximum i_{pc} value ($-0.517\ A\ cm^{-2}$), with the least onset potential ($-1.06\ V$), proving that it is the most effective coating for HER activity, compared to other coatings. The onset potential is defined as the potential at which the hydrogen evolution reaction commences. For this study, the onset potential of HER is obtained by the intersection of the extrapolated baseline current and the prolonged tangent of the cathodic linear curve. Moreover, the measured onset potential of the Ni–Mo–rGO electrode for HER was significantly more positive than that of the Ni–Mo electrode as shown in the comparison graph given in Fig. 8.

It is observed that at $-1.6\ V$, i_{pc} for HER decreases as the deposition c.d. increases and is approximately three times better than that of the binary Ni–Mo alloy coating. This increase in i_{pc} can be attributed to the increased electrochemically active surface area of the electrode, which is supported by the increased area covered under the CV plot. Therefore, it can be concluded that the Ni–Mo–rGO composite electrode displayed considerably higher electrochemical activity for hydrogen evolution and better electrocatalytic performance by reducing the overpotential of HER. Apparently, the enhanced performance of the Ni–Mo–rGO electrode towards electrocatalytic activity of HER in comparison with the Ni–Mo electrode is strongly credited to its chemical composition and microstructure.¹³

Chronopotentiometry

To test the electrocatalytic activity and stability of a catalyst, CP was utilized as a suitable technique. In this method, a controlled current (generally a constant current) is made to flow

between two electrodes, in which the potential of one electrode (working electrode) is monitored as a function of time with respect to a suitable reference electrode. The solution is usually, but not necessarily, unstirred and contains an excess of a supporting electrolyte so that diffusion is the principal mechanism of mass transport. Conventional industrial low-pressure alkaline electrolyzers usually operate at c.d.'s from $-100\ mA\ cm^{-2}$ to $-300\ mA\ cm^{-2}$.³⁴ Chronopotentiograms of the Ni–Mo–rGO composite coatings deposited at different c.d.'s along with the volume of H_2 gas liberated are shown in Fig. S4 (ESI[†]), for the initial 300 s. For all of the modified electrodes, the electrode potential reached a constant value after some time (Fig. S4, ESI[†]). It can be seen that the coating corresponding to $1.0\ A\ dm^{-2}$ shows the maximum liberation of H_2 (refer to Table 7), due to excess reduction of H^+ ions as there are plenty of active sites for their adsorption, provided by the graphene incorporated binary alloy matrix. This is further proved by the substantial reduction in the operating cathodic potential ($-1.51\ V$) of the Ni–Mo–rGO composite coating as compared to its binary alloy coating ($-1.74\ V$) as seen in Fig. 9. Also, the volume of hydrogen gas liberated in the first 300 s was found to be much higher in the case of composite coatings, as shown graphically in the inset of Fig. 9.

Mechanism for HER

The Tafel slope has often been used to identify the mechanism and rate-limiting step of HER. These characterization techniques revealed that the HER mechanism in high alkaline media consisted of the three following steps:³⁵

- electro-reduction of water molecules with hydrogen adsorption; Volmer reaction (eqn (3))
- electrochemical hydrogen desorption; Heyrovsky reaction (eqn (4))
- chemical desorption; Tafel reaction (eqn (5)).

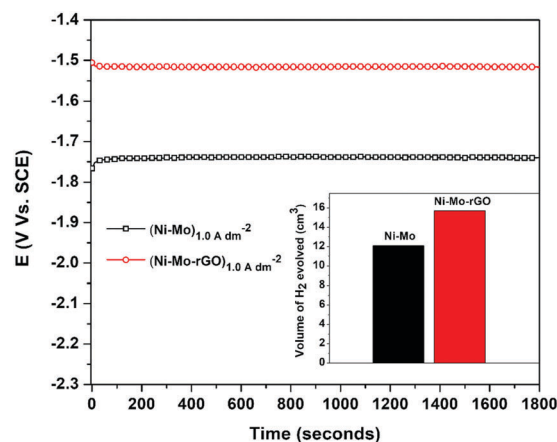
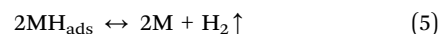


Fig. 9 CP curves at $-300\ mA\ cm^{-2}$ recorded for the Ni–Mo alloy and Ni–Mo–rGO composite coatings developed at $1.0\ A\ dm^{-2}$. The inset chart shows the volume of H_2 liberated in 300 s on each of the electrodes.

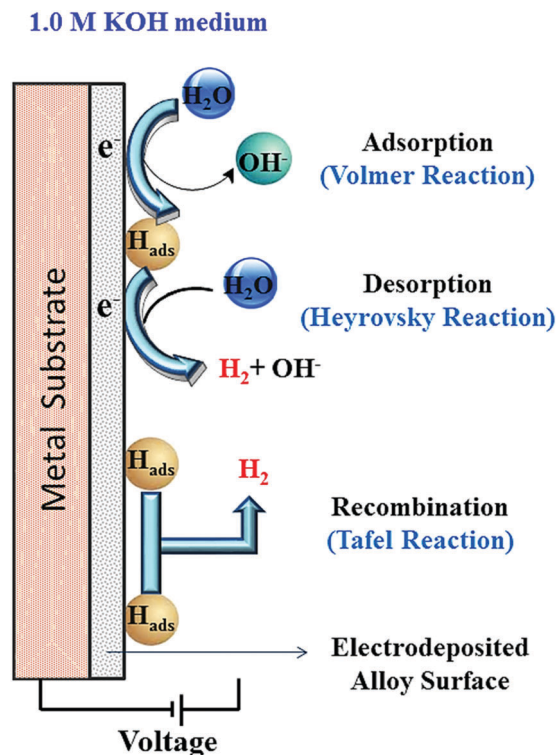


Fig. 10 Diagram showing the mechanism of HER on the surface of Ni–Mo–rGO composite coatings, used as the cathode respectively, in 1.0 M KOH solution.

The electrocatalytic HER on the Ni–Mo–rGO composite coatings can also be explained by means of a mechanism, as shown in Fig. 10. For a complete HER, the combinations of Volmer–Heyrovsky or Volmer–Tafel mechanisms should be involved to produce molecular hydrogen.

Tafel slope is an inherent property of a catalyst determined by the rate-limiting step of HER.³¹ The Tafel plots are shown in Fig. 6 and the corresponding β_c values are reported in Table 5. The Tafel slope for Ni–Mo–rGO was found to be around the theoretically obtained value of -118 mV dec^{-1} indicating that the rate-limiting step was the Volmer–Tafel mechanism (eqn (3) and (5)) being operative in the HER.³⁶ From the data obtained from Table 5, the composite deposited at 1.0 A dm^{-2} has the lowest β_c value compared to the rest of the composite coatings developed at a higher c.d. proving the fact that it is the more efficient electrocatalyst for HER. When compared with the binary alloy coating, the rGO induced Ni–Mo alloy shows better catalytic activity towards hydrogen production; this is because graphene acted as a communicating platform in facilitating the electron transfer and transport during the HER. As a result, the c.d. of the HER was enhanced. Therefore, the improved HER performances of the Ni–Mo–rGO composite coatings could also be attributed to the high specific surface area and excellent electrical conductivity of graphene present in the alloy matrix.³⁷

Conclusions

In this study, a simple electrochemical method was used to synthesize an electrocatalyst consisting of graphene.

The Ni–Mo–rGO composite coatings were electrochemically deposited on a copper electrode and characterized using different techniques in view of their possible applications as an electrocatalyst for an efficient hydrogen production in an alkaline solution. On the basis of the above experiments, the following conclusions are drawn:

- (1) The introduction of rGO into the Ni–Mo alloy matrix provided an abundance of available edge sites for HER.
- (2) With the highly exposed edge sites, the Ni–Mo–rGO film achieved an excellent electrocatalytic activity towards HER with a low η_c (-401.6 mV) and large i_0 (up to $4.31 \mu\text{A cm}^{-2}$).
- (3) The best coating exhibits a maximum i_{pc} of -0.517 A cm^{-2} at -1.6 V , which is approximately three times better than the binary Ni–Mo alloy.
- (4) Tafel slope analysis revealed that the HER on the surface of composite coatings follows the Volmer–Tafel mechanism.
- (5) The prepared Ni–Mo–rGO composite coating shows four times better corrosion stability in the alkaline medium than Ni–Mo alloy electrodes.
- (6) The highest electrocatalytic activity for the Ni–Mo–rGO composite coating is attributed to a synergistic effect between the binary alloy and rGO, in terms of its composition and increased surface area.

Conflicts of interest

There are no conflicts to declare.

Acknowledgements

Ms Sandhya Shetty acknowledges the National Institute of Technology Karnataka (NITK), Surathkal for the financial assistance in the form of an institute fellowship, and for the infrastructure used to carry out the present work.

References

- 1 C. J. Winter, *Int. J. Hydrogen Energy*, 2009, **34**, S1–S52.
- 2 T. N. Veziro and F. Barbir, *Int. J. Hydrogen Energy*, 1992, **17**, 391–404.
- 3 M. P. M. Kaninski, D. P. Saponjic, V. M. Nikolic, D. L. Zujic and G. S. Tasic, *Int. J. Hydrogen Energy*, 2011, **36**, 8864–8868.
- 4 C. Fan, D. L. Piron, A. Sleb and P. Paradis, *J. Electrochem. Soc.*, 1994, **141**, 382–387.
- 5 A. Kellenberger, N. Vaszilcsin, W. Brandl and N. Duteanu, *Int. J. Hydrogen Energy*, 2007, **32**, 3258–3265.
- 6 D. R. Kim, K. W. Cho, Y. Choi and C. J. Park, *Int. J. Hydrogen Energy*, 2009, **34**, 2622–2630.
- 7 J. M. Thomas and W. J. Thomas, *Principles and practice of heterogeneous catalysis*, John Wiley & Sons, Germany, 2nd edn, 2014.
- 8 E. Bełtowska-Lehman, *J. Appl. Electrochem.*, 1990, **20**, 132–138.
- 9 L. M. Rodriguez-Valdez, I. Estrada-Guel, F. Almeraya-Calderón, M. A. Neri-Flores, A. Martínez-Villafañe and R. Martínez-Sánchez, *Int. J. Hydrogen Energy*, 2004, **29**, 1141–1145.

- 10 D. E. Brown, M. N. Mahmood, A. K. Turner, S. M. Hall and P. O. Fogarty, *Int. J. Hydrogen Energy*, 1982, **7**, 405–410.
- 11 S. Harinipriya and M. V. Sangaranarayanan, *Langmuir*, 2002, **18**, 5572–5578.
- 12 Q. Han, S. Cui, N. Pu, J. Chen, K. Liu and X. Wei, *Int. J. Hydrogen Energy*, 2010, **35**, 5194–5201.
- 13 M. Xia, T. Lei, N. Lv and N. Li, *Int. J. Hydrogen Energy*, 2014, **39**, 4794–4802.
- 14 C. M. P. Kumar, T. V. Venkatesha and R. Shabadi, *Mater. Res. Bull.*, 2013, **48**, 1477–1483.
- 15 Q. Cheng, J. Tang, J. Ma, H. Zhang, N. Shinya and L. C. Qin, *Carbon*, 2011, **49**, 2917–2925.
- 16 J. Luo, S. Jiang, H. Zhang, J. Jiang and X. Liu, *Anal. Chim. Acta*, 2012, **709**, 47–53.
- 17 R. Ojani, R. Valiollahi and J. B. Raoof, *Energy*, 2014, **74**, 871–876.
- 18 Y. Zheng, Y. Jiao, Y. Zhu, L. H. Li, Y. Han, Y. Chen, A. Du, M. Jaroniec and S. Z. Qiao, *Nat. Commun.*, 2014, **5**, 3783.
- 19 Y. Li, H. Wang, L. Xie, Y. Liang, G. Hong and H. Dai, *J. Am. Chem. Soc.*, 2011, **133**, 7296–7299.
- 20 S. Shetty, M. M. J. Sadiq, D. K. Bhat and A. C. Hegde, *J. Electroanal. Chem.*, 2017, **796**, 57–65.
- 21 B. Subramanya, Y. Ullal, S. U. Shenoy, D. K. Bhat and A. C. Hegde, *RSC Adv.*, 2015, **5**, 47398–47407.
- 22 A. Marlot, P. Kern and D. Landolt, *Electrochim. Acta*, 2002, **48**, 29–36.
- 23 A. Brenner, *Electrodeposition of Alloys*, Academic Press, New York, 1963.
- 24 E. Chassaing, N. Portail, A.-F. Lev and G. Wang, *J. Appl. Electrochem.*, 2004, **34**, 1085–1091.
- 25 B. M. Jović, V. D. Jović, V. M. Maksimović and M. G. Pavlović, *Electrochim. Acta*, 2008, **53**, 4796–4804.
- 26 C. G. Vayenas, R. E. White and M. E. Gamboa-Aldeco, *Modern Aspects of Electrochemistry, Number 42*, Springer, New York, 2008.
- 27 M. Bratoeva and N. Atanasov, *J. Electrochem.*, 2000, **36**, 60–63.
- 28 J. M. Jakšić, M. V. Vojnović and N. V. Krstajić, *Electrochim. Acta*, 2000, **45**, 4151–4158.
- 29 S. Shetty and A. C. Hegde, *Metall. Mater. Trans. B*, 2016, **48**, 632–641.
- 30 E. Navarro-Flores, Z. Chong and S. Omanovic, *J. Mol. Catal. A: Chem.*, 2005, **226**, 179–197.
- 31 Y. Jiang, X. Li, S. Yu, L. Jia, X. Zhao and C. Wang, *Adv. Funct. Mater.*, 2015, **25**, 2693–2700.
- 32 R. Ojani, J. B. Raoof and E. Hasheminejad, *Int. J. Hydrogen Energy*, 2013, **38**, 92–99.
- 33 C. C. Hu and Y.-R. Wu, *Mater. Chem. Phys.*, 2003, **82**, 588–596.
- 34 G. S. Tasić, U. Lačnjevac, M. M. Tasić, M. M. Kaninski, V. M. Nikolić, D. L. Žugić and V. D. Jović, *Int. J. Hydrogen Energy*, 2013, **38**, 4291–4297.
- 35 F. Safizadeh, E. Ghali and G. Houlachi, *Int. J. Hydrogen Energy*, 2015, **40**, 256–274.
- 36 Y. Choquette, L. Brossard, A. Lasia and H. Menard, *J. Electrochem. Soc.*, 1990, **137**, 1723–1730.
- 37 Y. G. Huang, H. L. Fan, Z. K. Chen, C. B. Gu, M. X. Sun, H. Q. Wang and Q. Y. Li, *Int. J. Hydrogen Energy*, 2016, **41**, 3786–3793.